Biochimica et Biophysica Acta 1858 (2016) 1964–1973

Contents lists available at ScienceDirect

Biochimica et Biophysica Acta

journal homepage: www.elsevier.com/locate/bbamem

Analysis of neuronal nicotinic acetylcholine receptor α4β2 activation at the single-channel level

Camila Carignano, Esteban Pablo Barila, Guillermo Spitzmaul *

Instituto de Investigaciones Bioquímicas de Bahía Blanca, Universidad Nacional del Sur-Consejo Nacional de Investigaciones Científicas y Técnicas, B8000FWB Bahía Blanca, Argentina

ARTICLE INFO

Article history:
Received 7 March 2016
Received in revised form 9 May 2016
Accepted 16 May 2016
Available online 24 May 2016

Keywords:
Neuronal nicotinic receptor
Channel activation
Single-channel
Transfected cells
Kinetic modeling

ABSTRACT

The neuronal nicotinic acetylcholine receptor α4β2 forms pentameric proteins with two alternate stoichiometries. The high-sensitivity receptor is related to $(\alpha4)_2(\beta2)_3$ stoichiometry while the low-sensitivity receptor to $(\alpha4)_3(\beta2)_2$ stoichiometry. Both subtypes share two binding sites at the $\alpha4(^+)/\beta2(^-)$ interface with high affinity for agonists. $(\alpha4)_3(\beta2)_2$ has an additional binding site at the $\alpha4(^+)/\alpha4(^-)$ interface with low affinity for agonists. We investigated activation kinetics of both receptor subtypes by patch-clamp recordings of single-channel activity in the presence of several concentrations of acetylcholine (0.5 to 300 μM). We used kinetic software to fit these data with kinetic models. We found that the high-sensitivity subtype correlates with the low-conductance channel ($g_{-70} = 29$ pS) and does not activate with high efficacy. On the contrary, the low-sensitivity subtype correlated with a high-conductance channel ($g_{-70} = 44$ pS) and exhibited higher activation efficacy. Opening events of individual nAChRs at high agonist concentrations occurred in clusters, which allowed us to determine kinetic constants for the activation of the triliganded receptor. Our kinetic modeling identified an intermediate state, between resting and open conformation of the receptor. Binding of the third molecule increases the efficacy of receptor activation by favoring the transition between resting and intermediate state around 18 times. The low rate for this transition in the diliganded receptor explains the action of acetylcholine as partial agonist when it binds to the high-affinity sites. The presence of the third binding site emerges as a potent modulator of nicotinic receptor α4β2 activation which may display different functions depending on agonist concentration.

1. Introduction

Nicotinic acetylcholine receptors (nAChRs) are members of the ligand-gated ion channel (LGIC) superfamily together with the ionotropic γ-aminobutyric acid, serotonin and glycine receptors. They form pentameric receptors that open their intrinsic channels upon binding of neurotransmitters such as acetylcholine (ACh), serotonin, γ-aminobutyric acid (GABA) or glycine [1,2]. nAChRs mostly assemble as heteromers with a combination of at least 2 subunits, an α one that bear the principal binding site (BS) for the agonist ((+) face) and an accessory subunit that forms the complementary BS ((−) face), such as β, δ or ε subunits [1,3]. However, some receptors can also assemble as homomers, such as that formed by α7 or α9 subunits, where each subunit possesses the two faces of the BS [4]. Neuronal nAChRs can belong to either subgroup, being homomeric receptors represented only by α7 nAChR in the mammalian brain. Heteromeric mammalian neuronal receptors are assembled by at least 2 α subunits (from α2 to α6) and the complementary number of β subunits (from either β2 to β4) [2].

The predominant heteromeric neuronal nAChR expressed in the brain is the α4β2 receptor [5]. It is broadly expressed in CNS [6,7] and the physiological roles of this receptor subtype have been linked to attention, learning and memory [8,9] and in pathological processes such as nicotine addiction, autosomal nocturnal frontal epilepsy and neurodegenerative disorders [1,10,11]. nAChRs are localized post- and presynaptically and also in the preterminal area. In the last two regions, they would perform the main physiological functions [1,6,9,12]. Here, nAChRs modulate the release of several neurotransmitters directly or indirectly [13–17].

nAChR α4β2 was found to be expressed with two different stoichiometries, containing 3 α4 and 2 β2 subunits ($(\alpha4)_3(\beta2)_2$) and conversely ($(\alpha4)_2(\beta2)_3$) [18–20]. Each stoichiometry has different sensitivities for agonists, with high-sensitivity (HS) and low-sensitivity (LS) receptors associated with $(\alpha4)_2(\beta2)_3$ and $(\alpha4)_3(\beta2)_2$ stoichiometries, respectively. These subtypes have in principle two structurally equivalent BSs located at the interface between α4 and β2 subunits ($\alpha4^{(+)}/\beta2^{(-)}$) with high-affinity for the agonist ACh [21], although

Abbreviations: ACh, acetylcholine; BS, binding site; HC, high-conductance; HS, high-sensitivity; LC, low-conductance; LS, low-sensitivity; nAChRs, nicotinic acetylcholine receptors.

* Corresponding author at: Instituto de Investigaciones Bioquímicas de Bahía Blanca, UNS-CONICET, Camino la Carrindanga Km 7, B8000FWB Bahía Blanca, Argentina.
E-mail address: gspitz@criba.edu.ar (G. Spitzmaul).

http://dx.doi.org/10.1016/j.bbamem.2016.05.019
0005-2736/

would not be functionally equivalent [22]. The structural basis for the differences in sensitivity was found to be located in an additional BS for agonists that is present only in $(\alpha4)_3(\beta2)_2$ subtype [21,23]. This stoichiometry has and $\alpha4^{(+)}/\alpha4^{(-)}$ interface, that binds the natural agonist ACh with lower affinity than the canonical site $\alpha4^{(+)}/\beta2^{(-)}$ but improves channel activation.

Due to differences in agonist sensitivity and receptor subtype localization in some cases, it is supposed that both subtypes would perform different functions [9]. HS subtype mediates glutamate release in prefrontal cortex and striatum [17,24–26] but also LS subtype has been implicated in this function in the prefrontal cortex [26]. Using the LS site-selective agonist NS9283 [27], it was demonstrated that this subtype participates in cognitive function and analgesia, opening the possibility to use this kind of drugs as cognitive enhancers in patients with Alzheimer disease or neuropathic pain [28,29].

We used transiently transfected cells with the α4β2 receptor to study activation kinetic of receptor subtypes by analysis of single channel recordings. Our results link channel conductances with receptor stoichiometries and activation kinetic. $(\alpha4)_2(\beta2)_3$ subtype has lower unitary conductance with a pattern of channel activation with low-efficacy. On the contrary, $(\alpha4)_3(\beta2)_2$ channel has a higher conductance and a higher opening efficacy. Binding of ACh to the 2 high-affinity BS does not generate an efficient coupling to gating but binding of the third molecule to the low-affinity BS does. Our kinetic analysis suggests the presence of primed states, as demonstrated for others receptors of the Cys-loop family [30–33], that precede channel opening and that limits activation efficacy for either subtype.

2. Materials and methods

2.1. Expression of neuronal nAChRs

Total mRNAs were extracted from mouse brain and cDNA for α4 and β2 nAChR subunits were obtained using specific primer pairs. cDNAs were cloned into pcDNA3.1 (Invitrogen, cat N°V790-20) vector using restriction enzymes *Eco*RI/*Xho*I for both nAChR subunits. BOSC cells, a cell line derived from HEK cells which increase protein expression [34], were transfected with a total amount of 5 μg of plasmid DNAs containing neuronal α4 and β2 subunits in a ratio 1:1 using the calcium phosphate precipitation method [35]. To check for different stoichiometries assembly, we also transfected the subunits in a 1:4 or 4:1 ratio. To identify transfected cells, a plasmid encoding green fluorescent protein was included in the cDNA mixture diluted ten folds of the total 5 μg cDNA. For transfections, cells at 40–50% confluence were incubated for 8–12 h at 37 °C with the calcium phosphate precipitate containing the cDNAs in DMEM plus 10% fetal bovine serum. Cells were used for recordings 2 to 3 days after transfection.

2.2. Patch-clamp recordings

Single-channel currents were recorded in the cell-attached configuration at 22 °C. The bath and pipette solutions contained an equimolar depolarizing solution composed of (in mM): 142 KCl, 5.4 NaCl, 0.2 $CaCl_2$ and 10 HEPES, pH 7.4. In this condition, membrane potential was close to 0 mV. Pipette potential applied was +70 mV. ACh was added to the pipette solution at different concentrations. Pipettes were pulled from capillary tubes and coated with Sylgard. Single-channel currents were recorded using an Axopatch 200B amplifier (Molecular Devices), low-pass filtered to 5 kHz, digitized at 10 us intervals with the PCI-6111E interface (National Instruments, Austin, TX), recorded to the computer hard disk using the Acquire program (Bruxton Corporation, Seattle, WA). Recordings were manually analyzed outline using the TAC X4.2.0 software (Bruxton Corporation) at a final bandwidth of 5 kHz. Channels were observed as upward deflections from the baseline and analyzed individually for amplitude, open- and closed-time durations. Open- and closed-time histograms were plotted by using a logarithmic abscissa and a square root ordinate and fitted to the sum of exponential functions by maximum likelihood using TACFit X4.2.0 software (Bruxton Corporation). To determine amplitudes corresponding to different assembly stoichiometries, opening events were tracked individually without any amplitude restriction. Then we constructed amplitude histograms and mean amplitude values for different populations were determined by fitting with Gaussian functions. We used at least 3 different recordings from the transfected cells to determine the mean ± S.E. for each amplitude population. From the fitted histograms, we also determined manually the intersection point between the 2 amplitude populations, which corresponded to the value where both curves intersected each other (see Fig. 2B). This method generated misclassified events that corresponded to the overlapping region under the fitted curves (Fig. 2). The fraction of misclassified events was on average 8 ± 3% of total events. To determine the mean open- and mean closed-duration for each low-conductance (LC) and high-conductance (HC) channel amplitudes we used the opening events detected in the analysis performed without any restriction. Then we constructed open-time and closed-time histograms for either LC or HC channels by selecting the openings and closed events that occur in between an amplitude range below and above the intersection point, respectively.

2.3. Kinetic analysis

Kinetic analysis was performed as described before [36,37]. The analysis was restricted to clusters of channel openings, each reflecting the activity of a single nAChR. Clusters were identified as a series of opening events preceded and followed by closed intervals longer than a critical duration (ι_{crit}), which was taken as the point of intersection of the concentration-dependent closed component (τ_{cl3}^{HC}) and the succeeding one in the closed-time histogram. ι_{crit} changed with ACh concentration. For lower concentrations of agonist we observed a high degree of overlapping events between τ_{cl3}^{HC} and the succeeding one, which difficulted determination of ι_{crit}. However, at higher agonist concentrations, as τ_{cl3}^{HC} shortened, ι_{crit} was more accurately determined. Average value for misclassified closed events was 7 ± 4 of the total events observed in clusters in the range of 50 to 300 μM ACh. Clusters showing double openings were rejected. Typically more than 80% of the clusters were selected [36]. The resulting open and closed intervals were analyzed according to kinetic schemes using QuB software (www.qub.buffalo.edu, State University of New York, Buffalo) [38]. The dead time was 50 μs. The model and the estimated rates were accepted if the resulting probability density functions correctly fitted the experimental open-duration and closed-duration histograms.

3. Results

3.1. Identification of opening events elicited by neuronal nAChRs α4β2

In order to analyze α4β2 nAChRs activation, we performed single-channel recordings on transiently transfected BOSC cells with cDNA for both subunits in a ratio 1:1. Recordings were done in the presence of ACh concentrations from 0.5 to 300 μM. Initially, to identify nAChRs channel openings, recordings were done in untransfected cells in the presence of 50 μM ACh in the pipette; and transfected cells without ACh in the patch pipette. In these conditions and at a pipette potential of +70 mV, no channel activation was observed, or in the case of transfected cells, infrequently isolated openings of 3–4 pA were observed with a total open-time fraction < 0.01. Occasionally, in untransfected and transfected cells (with or without ACh in the pipette solution), opening events with an amplitude of 5 pA were observed. They activated as consecutive openings of about 1 ms separated by a closed time of approximately 100 μs and the activity did not decay over time. This channel activation was consistent with the already observed endogenous channels that are expressed in HEK cells, the

original cell line which gave rise to BOSC cell line [39,40]. When this channel appeared during recording the data was discarded. In the presence of ACh, in transfected cells, we observed a consistent activation of opening events of around 3 to 4 pA that we identified as events generated by activation of the nAChRs. As previously reported by others, characterization of this nAChR activation is complicated because of deep desensitization of the receptor in the continuous presence of agonists or run-down [18,41–43]. The probability of getting single-channel currents in the presence of ACh was below 0.2 (1 successful patch every 6/7 patches). In successful patches, in most of the cases, channel opening events decayed within the first 2 min after sealing (Fig. 1A) with a low proportion of recordings that exhibited a reasonable activity for 5 to 10 min. In any case, the total number of opening events was never above 1500 with a media of 400 events ($n = 76$). The frequency of channel openings increased with ACh concentration (Fig. 1B). At the lowest ACh concentration (0.5 μM), the frequency of channel openings was below 0.2 and increased 7-fold when 100 μM ACh was present in the pipette (Fig. 1C). Thus, the concentration-dependence, together with the detection of these channels only in transfected cells, supported initially our idea that these events were generated by the activation of nAChRs. Additionally, we transfected cells with different amount of cDNA ratios which changed the proportion of the populations observed and we also noticed changes in the activation kinetic (see below).

3.2. Characterization of nAChRs α4β2 single-channel opening events

Once we identified opening events corresponding to the transfected neuronal nAChRs, next we analyzed the amplitude and activation parameters of these channels. As also reported by others [18,41–46], we found two different channel amplitudes at all concentrations of ACh, a low-conductance (LC) channel of around 2 pA and a high-conductance (HC) channel of around 3 pA (Fig. 2A and B). Both amplitudes didn't change significantly with increasing concentrations of ACh ($p > 0.05$, ANOVA test) (Fig. 2B and C, left panel). So, we pooled the amplitude values at all concentrations and obtained an average value of 2.09 ± 0.19 pA ($n = 23$) for the LC channel and 3.14 ± 0.28 pA ($n = 24$) for the HC channel. The chord conductances (g_{-70}) for the LC and HC channels were 29 ± 3 pS and 44 ± 4 pS, respectively. The number of events in each population of channel changed with ACh concentration (Fig. 2C, right). At 0.5 μM ACh, the relative area for the LC component was around 0.6 and decreased to a value below 0.4 at concentrations ≥ 10 μM ACh while HC component increased to values ranging between 0.65 and 0.9 (Fig. 2C). We also evaluated channel amplitudes of cells transfected with cDNAs ratios of 4:1 and 1:4 for α4 and β2, respectively. We evaluated channel properties of the receptors activated by 30 μM ACh. We observed both channel amplitudes that were similar to the 1:1 ratio (for 4:1 ratio: 2.02 ± 0.22 ($n = 4$) and 3.24 ± 0.15 ($n = 6$); for 1:4 ratio: 2.15 ± 0.22 ($n = 4$) and 3.02 ± 0.25 ($n = 4$)). However, we determined a change in the distribution of channel populations. With a 4:1 ratio, mostly all openings were HC channels with a relative area of 0.92 ± 0.04 ($n = 4$). The opposite was observed for the 1:4 ratio, LC channel were more frequent and predominated in the histogram (relative area: 0.86 ± 0.06) but the number of opening events was lower compared to the other transfection ratios. In consequence, data from several patches were pooled.

Next we analyzed the duration of the opening events (Fig. 3). Initially, we used the raw data obtained from the data analysis without discriminating between LC and HC channels. Open time histograms showed two mean open time components, a short-duration component (τ_{on1}) of about 500 μs that did not change significantly with ACh concentration and a long-duration component (τ_{on2}) that changed with increasing concentration of ACh from 2 ms at 10 μM ACh to 1 ms at 300 μM ACh ($p < 0.05$). To determine if each component corresponded to LC and HC channels and gain more insights into the channel activation of each population, we sorted open-time durations for LC and HC channels and generated open-time histograms for each category (see Materials and methods). For both populations, we observed a short and a long open-time component at all ACh concentrations (Fig. 3A and B). For the LC channel, the duration of both components did not change with ACh concentration ($p = 0.81$ and $p = 0.98$, respectively; ANOVA's test). Mean open time for the short component (τ^{LC}_{on1}) at all concentration was 0.26 ± 0.03 ms (S.E., $n = 21$) and for the long component (τ^{LC}_{on2}) was 1.31 ± 0.14 ms (S.E., $n = 21$). τ^{LC}_{on1} was the predominant component at all concentrations with a contribution above 0.7 of the relative area (Fig. 3C). For the HC channel, we obtained also 2 open components, a short (τ^{HC}_{on1}) and a long component (τ^{HC}_{on2}). τ^{HC}_{on1} changed slightly but significantly the open-time duration from 10 to 300 μM ACh ($p = 0.02$, Student's *t*-test). Except for 300 μM, τ^{HC}_{on1} was longer than τ^{LC}_{on1} ($p < 0.01$, Student's *t*-test), indicating different activation kinetic. τ^{HC}_{on2} decreased slightly but not significative from 10 to 100 μM ACh (Fig. 3C) ($p = 0.45$, respectively; ANOVA's test). However, at 300 μM ACh, the presence of this component was not constant. In 2 of the 3 recordings obtained for this concentration, only one exhibited this component and the rest had only 1 brief component. This concentration is shown in Fig. 3C, but only for 1 recording. Average τ^{HC}_{on2} (10 to 100 μM ACh) was 1.32 ± 0.14 ms (S.E.; $n = 15$). The duration of the long component of LC and HC channels did not differ significantly ($p = 0.6$; Student's *t*-test). For both channel populations, the predominant open component was the short one (Fig. 3C, right panel). However, the behavior with ACh concentration differed between both populations. While the relative area of τ^{LC}_{on1} remained

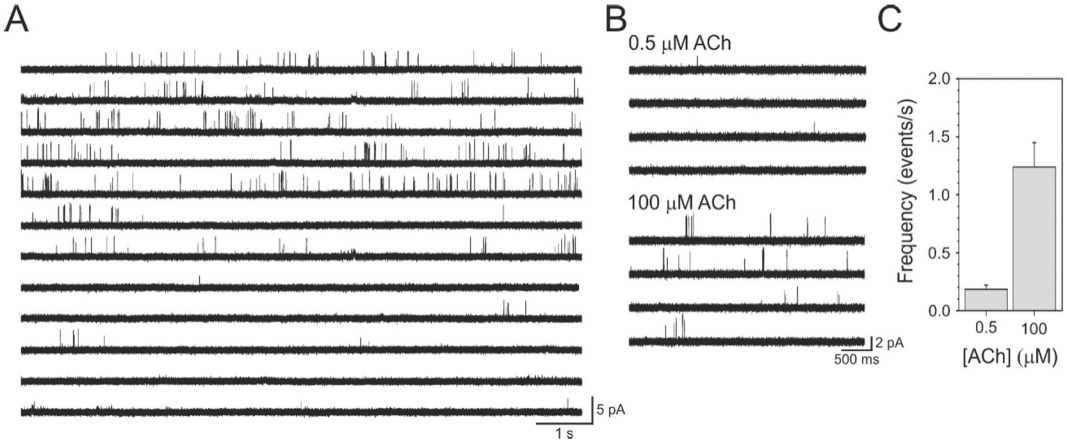

Fig. 1. Activity of nAChR α4β2 activated by acetylcholine in cell-attached recordings of transiently transfected BOSC cells. (A) Continuous single-channel recording of the neuronal subtype receptor activated by 100 μM ACh. Openings are shown as upward deflections. (B) Activity of opening events at two different ACh concentrations. (C) Average frequency of channel openings at the indicated concentrations of ACh. $n = 7$ and $n = 6$ for 0.5 and 100 μM ACh, respectively. Pipette potential for all recordings: +70 mV.

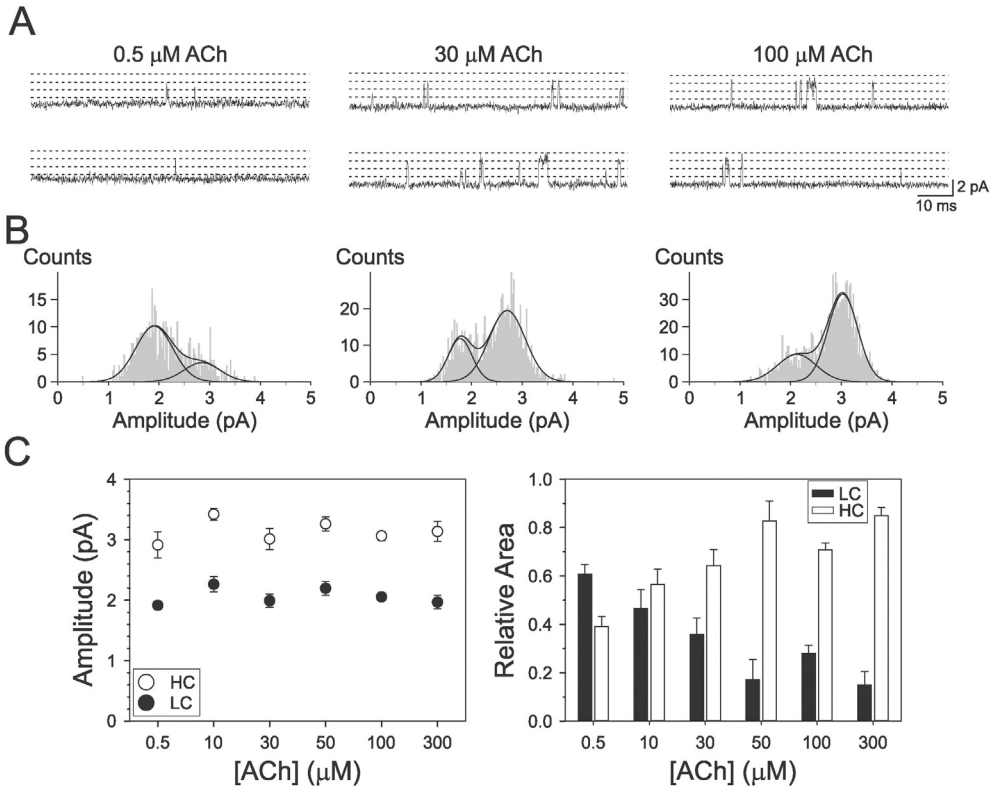

Fig. 2. Characterization of single-channel opening events. (A) Opening events elicited by different concentrations of ACh. Dash lines indicate 1 pA of amplitude. (B) Opening histograms corresponding to recordings shown in A. Graphs were fitted with 2 components. (C) Average values obtained for the amplitudes (left) and relative area (right) obtained from the fitted histograms at different concentrations of ACh. Values are shown as average ± S.E. Two channel amplitudes were found and named "low-conductance" (LC) and "high-conductance" (HC) channels. All recordings were obtained at +70 mV pipette potential.

constant with ACh concentration (Fig. 3C, right; $p = 0.35$, ANOVA's test), the relative area of τ_{on1}^{HC} increased significantly with agonist concentration (Fig. 3C, right).

Additionally, we analyzed closed-time periods for both populations (Fig. 4). LC channel exhibited mostly isolated opening events (Fig. 4A) and occasionally it was observed as 2–3 consecutive openings. For this reason, closed-time histograms showed a variable number of long components that varied among recordings (Fig. 4B, left). The durations of these closed components were dependent on the number of channels present in the patch pipette and corresponded to the period in which LC channel receptors stayed in desensitized states. Activity of the channel is observed when they returned from desensitized states. The shortest component was more constant with a mean closed duration around 100 μs, independently of ACh concentration and the relative area of this component did not modify with the agonist concentration (around 0.25, not shown). Activation of HC channel deeply differed from LC channel. HC channel opened as burst of consecutive openings (Figs. 4A and 6A). Closed time histograms for HC channel indicated 2 components whose durations were independent of ACh concentration ($p = 0.32$ and $p = 0.48$, respectively). These corresponded to the 2 shortest components (τ_{cl1}^{HC} and τ_{cl2}^{HC}; Fig. 4B, close-arrow). Average values were 0.13 ± 0.01 ms for τ_{cl1}^{HC} and 1.91 ± 0.10 ms τ_{cl2}^{HC}. Besides, the contribution of these components increased significantly with the agonist concentration (Fig. 4B and C, right panel), indicating a dependence of activation kinetic with agonist concentration. Additionally, we observed a third closed component (τ_{cl3}^{HC}), longer than τ_{cl2}^{HC} that shortened with increasing concentrations of ACh (Fig. 4B, open-arrow). The intersection between this concentration dependent component and the succeeding one was taken to define clusters (Fig. 4B). At 100 μM ACh the component had an average value of 27.98 ± 2.48 ms (Fig. 4B) (SE, $n = 18$). Longer closed-components were more variable among ACh concentrations, indicating periods in which HC channels enter in long-lived desensitized states. Durations of these long closed components depends on the number of HC channels present in the patch pipette and are not useful for kinetic analysis. Return from desensitization allowed channel to activate in bursts and clusters (Fig. 6A). For these reasons, long shut periods were discarded for kinetic analysis.

3.3. Determination of activation kinetic parameters

Once we characterized activation parameters for open and closed components, we assigned the activation of LC and HC channels to the 2 possible stoichiometries based on the results shown previously (see Discussion): LC channel corresponded to the high-sensitivity $(\alpha4)_2(\beta2)_3$ receptor (Fig. 5A, left), meanwhile, HC channel correlated with the low-sensitivity receptor $(\alpha4)_3(\beta2)_2$ (Fig. 5A, right). LC channel would activate according to Scheme 1 (Fig. 5B), in which two agonist molecules can bind to the high-affinity BS (Fig. 5A, white arrows). HC channel also has the two high-affinity BS structurally identical to LC channel and, additionally, the third low-affinity BS located in the $\alpha4(^+)/\alpha4(^-)$ face (Fig. 5A, black arrow). Thus, HC channel would activate at low concentrations of ACh by binding to the 2 HA sites and when agonist concentration is increased, it will bind to the third site (Fig. 5B, Scheme 2).

In order to analyze the kinetic of activation of nAChRs, we used our experimental single-channel data to test models of channel activation. Due to the lack of activation in clusters for LC channel, it was not possible to analyze kinetic behavior for this channel. So, we performed this analysis only for HC channel. In typical cell-attached recordings, clusters of events were easily detected at a low temporal resolution as series of opening events that occur after long shut periods (Figs. 1 and 6A). Detailed observation of clusters activity at higher temporal resolution showed that opening events occurred in between an irregular pattern of closing periods (Fig. 6A). Initially, it is possible to identify openings

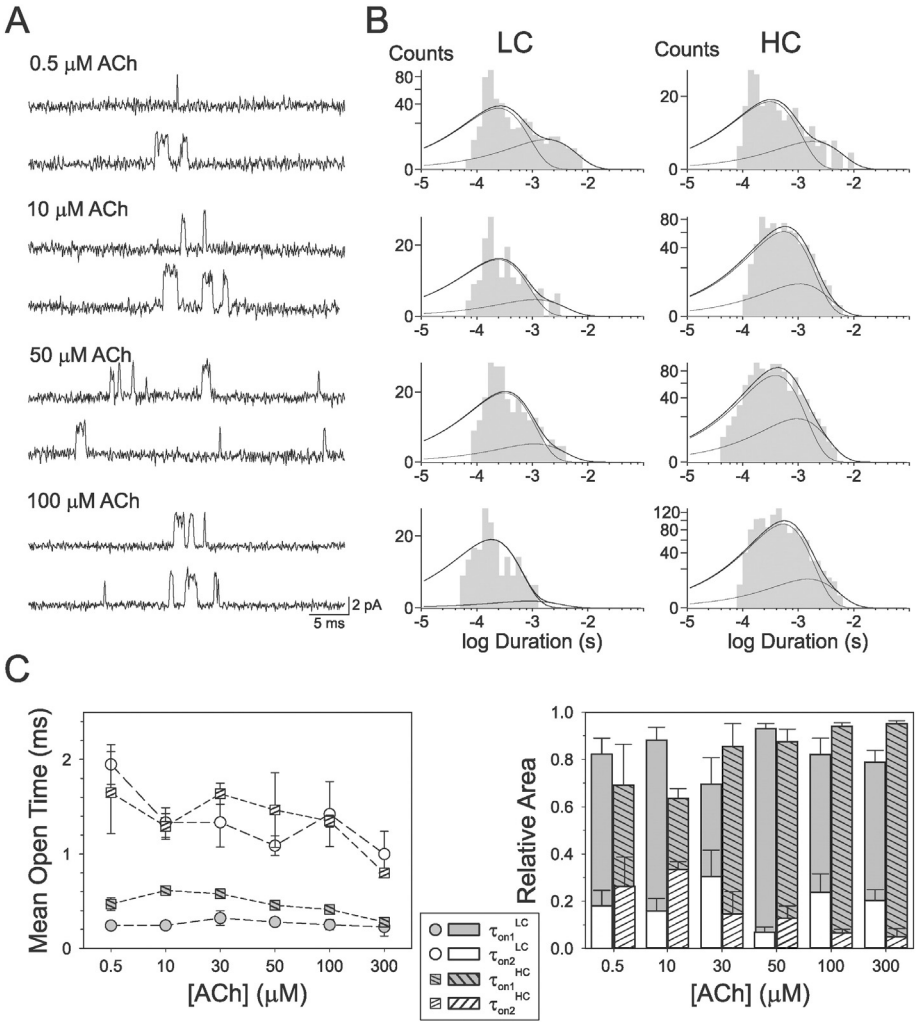

Fig. 3. Analysis of the duration of opening events for LC and HC channels. (A) Single-channel recordings showing channel duration at different concentration of agonist. (B) Open time histograms for LC and HC channels for the corresponding recording shown in A. Channel populations were split according to amplitude histogram as explained in Materials and methods. (C) Average values for the mean open time (left) and relative area (right) obtained for the two components of LC and HC channels from the open histograms. Values are shown as mean ± S.E.

events separated by very short closing periods (bursts). These bursts within clusters are separated by longer closing periods (Fig. 6A, high) and also individual openings in between bursts activity (Figs. 4A and 6A). Closed time from the bursts activity accounts for the shortest closed-time components (Fig. 4B).

For kinetic analysis, we assumed that as for LC channel, binding of ACh to the high-affinity sites did not render channel activation in clusters behavior and, in consequence, clusters are generated by the increased efficacy of channel opening when the third ACh molecule binds to the LA site [47]. So, we constrained our analysis only to the last step of the proposed model of channel activation (Fig. 5B, dash line in Scheme 2). We fitted channel activation to several models based on that derived from Scheme 2 (Fig. 5B and C) using the Maximum Interval Likelihood (MIL) algorithm from the QuB suite. Models 1 and 2 possess a transition from diliganded resting state to the corresponding open state, a transition that is expected to take place in HC channel, as isolated events are present at very low concentrations of agonist. However, fitting of experimental data to kinetic schemes with MIL program did not render a rational value for this transition. Closing constants α_2 were extremely low, which in consequence resulted in very high gating constants for diligated receptors (Table 1). This is not compatible with the observed kinetic behavior, for example at low ACh concentrations. Besides, the goodness of fit for Models 1 and 2 were the lowest (Log-likelihood (LL) ~85,900 for both models). Models 3 and 4 lacked this transition and fitting of kinetic values were improved (Table 1, LL 85900 and 102,700 for Models 3 and 4, respectively). However, as explained before, we expected that this transition would take place. Additionally, as desensitization from diligated open state should be a long-lived state, we excluded this state from fitting (Models 2 and 4). For Model 2, the lack of this state did not change fitting obtained using Model 1. For Model 4, fitting is slightly improved compared with Model 3. However, the main problem for the kinetic models was the lack of transition in the diligated state. Thus, all these models gave us values that didn't fit properly the expected kinetic behavior of channel openings (Table 1).

It has been demonstrated that LGIC can exhibit intermediate closed states between agonist-bound resting and opening states, named flipped and also primed state [30–32,48,49]. We analyzed this possibility for the receptor by evaluating a model that included a closed primed state between diliganded and triliganded state and the corresponding open states (Fig. 6B). The third agonist molecule binds to either diliganded closed-, flipped- or open-state or dissociate from the corresponding triliganded state. For the analysis we excluded desensitized state occupied by 2 ACh molecules because we assumed that it is a long lived state. We fitted our experimental data to Model 5 shown in bold letters (Fig. 6B). Open-time and closed-time histograms at several ACh concentrations are well described by the theoretical curves (Fig. 6C), indicating that Model 5 describes well kinetic behavior of HC

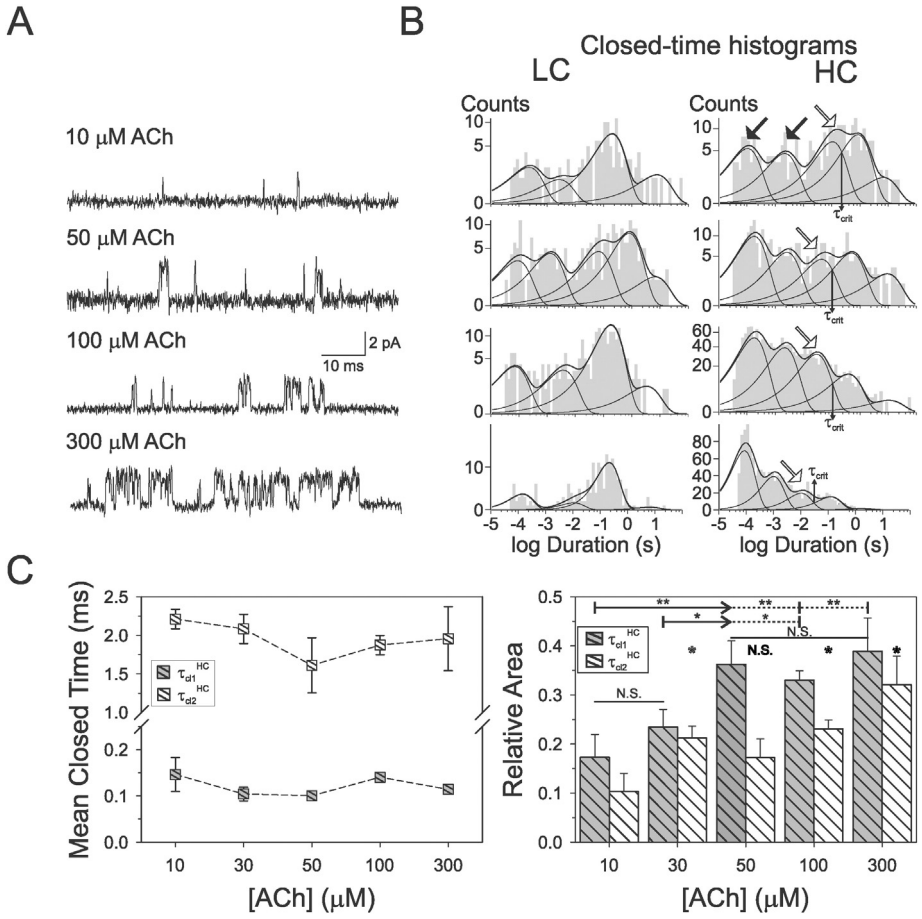

Fig. 4. Closed-time analysis for LC and HC channels. (A) Single channel recordings at different ACh concentrations. (B) Closed-time histograms corresponding to the recordings shown on the left. Closed-periods were split for LC and HC channel as explained in Materials and methods and fitted as the sum of exponential functions. Black arrows on top indicate concentration-independent components, named τ_{cl1}^{HC} and τ_{cl2}^{HC}, respectively for all histograms. White arrow indicates concentration-dependent component τ_{cl3}^{HC}. Intersection of this component and the succeeding one was used to determine τ_{crit}, which is indicated by thin arrows. (C) Average mean values for the two components indicated in B. Left, mean closed time and right, relative area at each concentration obtained from the corresponding histograms.

receptor. Association rates for the third agonist molecule to the resting state gave an equilibrium constant (K_3) value closed to 100 μM, similar to the EC_{50} reported for the LS receptor. Interestingly, transition rates to the primed state from the resting states A_2R and A_3R greatly differ, exhibiting an 18-fold increase in equilibrium constant from the triliganded state (F_3) compared to the diliganded state (F_2) (Table 1). Based on the rate constant obtained (Table 1), once the receptor reached the diliganded state, it had two possibilities. At concentrations of ACh below 15 μM, the transition to the diliganded flipped state is favored. However, when ACh concentrations increased above this value, the association of the third molecule increased transition to the triliganded resting state and the transition to the triliganded primed state. Surprisingly, activation constants are higher for diliganded than triliganded state (θ'_2 and θ'_3, Table 1), indicating that transition from the flipped state to the open state is not the limiting rate for the channel to open (Table 1). Model 5 shows 2 open states in which, according to constant rates, the shortest one corresponds to the triliganded state A_3O'. The long one corresponds to the diliganded state, A_2O'. At high ACh concentrations, when the triliganded open state is favored, reaching A_2O' state will proceed mainly from the unbinding of ACh molecules from the triliganded states, either A_3R' or A_3O'. The first one generates a closed time that precedes diliganded gating. The second one prolongs the open duration, that will finish by closing the diliganded state. According to Model 5, the unbinding/binding step of the primed state (K'_3) is very unlikely and the transition between open states is more probable (J'_3) (Table 1). In order to test if the transition between primed states is possible, we generated Model 6 in which we excluded the transition between open states, forcing the program to assign kinetic values to this parameter (Table 1). Model 6 rendered values similar to that of Model 5, but with much higher values for kinetic constants for k'_{+3} and k'_{-3}. In consequence, with this model, the transition between primed states is also possible and the goodness of fit is exactly the same as Model 5 (not shown).

4. Discussion

We studied the activation kinetic at the single channel level of neuronal nAChRs α4β2, which assembles with two different stoichiometries, with the patch-clamp technique. Our results showed the differences in activation performed for each receptor subtype and provide an explanation for the partial agonism exhibited by the receptors activated at the high-affinity BSs and how the third agonist molecule, acting at the low-affinity BS improved activation.

4.1. Stoichiometry and conductance

In single channel recordings of transfected cells, we determined two conductances for channel openings, a low-conductance channel with a chord conductance of 29 pS and a high-conductance channel with 44 pS (Fig. 2). Our values are in the range already published using different species and techniques [18,41,43–45,50–55]. Most of them observed 2 conductances and even 3 different ones. The structural basis for the two conductances would be determined by differences in channel assembly. In this regard, two stoichiometries have been proposed

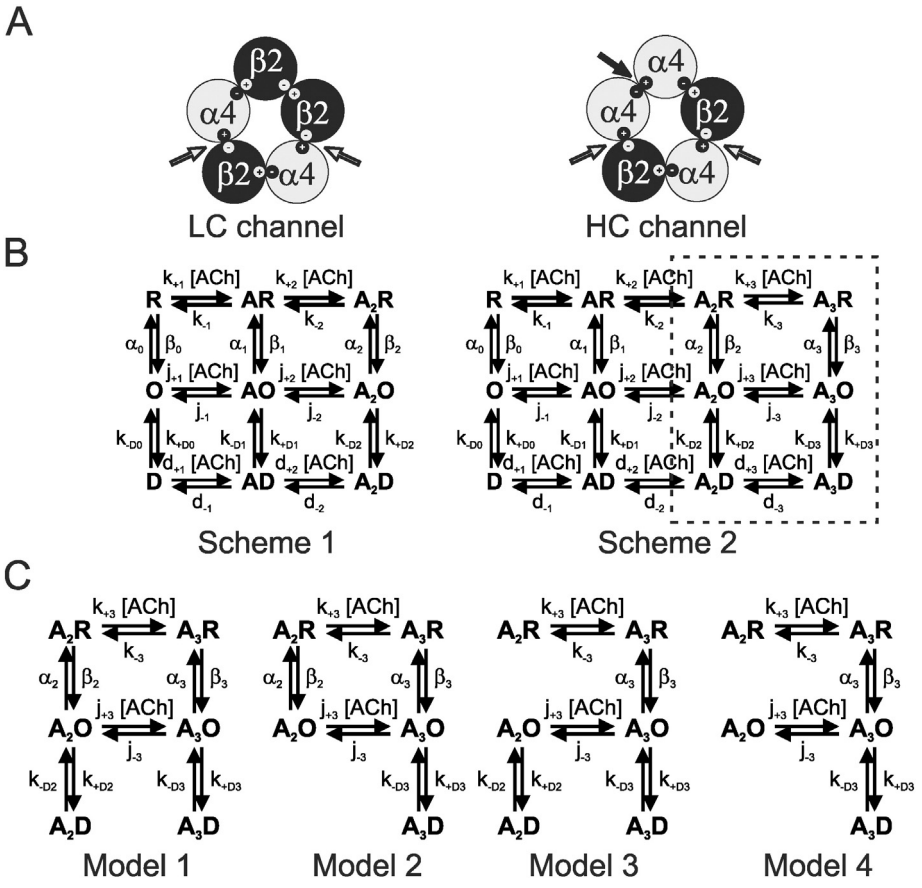

Fig. 5. Schematic representation of LC and HC channels activation. (A) Scheme of the LC and HC channels assembly. (B) Kinetic diagram for either channel activation according to the number of binding sites. Dash line on Scheme 2 indicates the binding step of the third ACh molecule and was used to model HC channel kinetic of activation. (C) Models for HC channel activation used to fit experimental data using QuB software.

for this receptor subtype based on agonist sensitivity, a high- and a low-sensitivity receptor that differs in the number of α4 and β2 subunits present in the pentamer [18,19,45]. The high-sensitivity receptor was associated with $(\alpha4)_2(\beta2)_3$ stoichiometry meanwhile low-sensitivity receptor with $(\alpha4)_3(\beta2)_2$ stoichiometry. Both assemblies were validated by experiments done with concatameric subunits which confirmed the relationship between stoichiometry and agonist sensitivity [20,21,23]. Based on our results, we assigned the activation of LC and HC channels to the 2 possible stoichiometries: LC channel corresponds to the high-sensitivity receptor $(\alpha4)_2(\beta2)_3$, meanwhile HC channel correlates with the low-sensitivity receptor $(\alpha4)_3(\beta2)_2$. Our conclusions are based on the following findings: a) Activity of channel openings increased with ACh concentration, where LC channels are predominant at very low concentration and their contributions decrease with increasing concentration of agonist. The opposite was determined for HC channel; its contributions are minor at 0.5 μM ACh and predominate at higher concentrations. b) Transfection with α4 and β2 cDNA in a ratio 4:1 increases the proportion of HC channels while transfection with a ratio 1:4 increases the proportion of LC channel. c) HC channel activity at high agonist concentration occurs in clusters, indicating a higher activation efficacy, which was previously found for the low-sensitivity subtype [43,47]. Similar conclusions were reported by two groups using either single-channel or noise-analysis [18,43]. However, the opposite conclusion was obtained by [45]. Channel conductance of the Cys-loop superfamily depends on the transmembrane domain 2 (TM2), which lines the channel pore, and also on a cytoplasmic helix formed by the TM3–TM4, named MA-stretch, which forms intracellular portals that the ions must cross when entering or leaving the cytoplasm [56]. Residues present in this region are important to determine channel conductance of α4β2 receptors [57]. Structurally, the 5 portals formed by the interface between MA regions in α4β2 receptors would differ between receptor subtypes. LC and HC channels have in common 2 α4/β2 and 2 β2/α4 portals but LC channel has a β2/β2 portal meanwhile HC channel has an α4/α4 portal. Differences in the structure of these portals could account for the different conductances observed for LC and HC channels, taking into account that the key residues in TM2 for channel conductance are conserved between both subunits.

4.2. Activation and efficacy

We found that the LC channel did not activate in clusters, whereas the HC channel did. Opening in clusters that correspond to the same receptor molecule flickering in between different states [38], indicates a better gating efficacy [58–60]. $(\alpha4)_2(\beta2)_3$ receptor has two identical BSs at the $\alpha4^{(+)}/\beta2^{(-)}$ interface that, according to sensitivity and mutation analysis of concatamers, has high-affinity for ACh (EC_{50} ranged between 0.95 and 3.8 μM). $(\alpha4)_3(\beta2)_2$ assembly introduce an additional BS at the $\alpha4^{(+)}/\alpha4^{(-)}$ interface, with low-affinity for ACh (EC_{50} ranged from 80 to 130 μM) [18–21,23,47]. Despite this affinity profile, the efficacy of activation upon binding of the agonist to the high- or low-affinity sites is opposed. Binding of ACh to the high-affinity BS generates gating of the channel but, maximal activation of the $(\alpha4)_3(\beta2)_2$ is achieved when ACh concentration raises, allowing binding to the third site [21,23,47,61,62]. LC channel would activate according to Scheme 1 (Fig. 5B), in which 2 agonist molecules can bind to the high-affinity BS, $\alpha4^{(+)}/\beta2^{(-)}$. As we could not detect clusters for this channel although binding occurs with high-affinity, gating efficacy must be low, with ACh acting as a partial agonist, as already reported [22,27,47,61,62]. In this regard, $(\alpha4)_3(\beta2)_2$ subtype, when activated by the high-affinity BSs, accounts for approximately a 20% of the

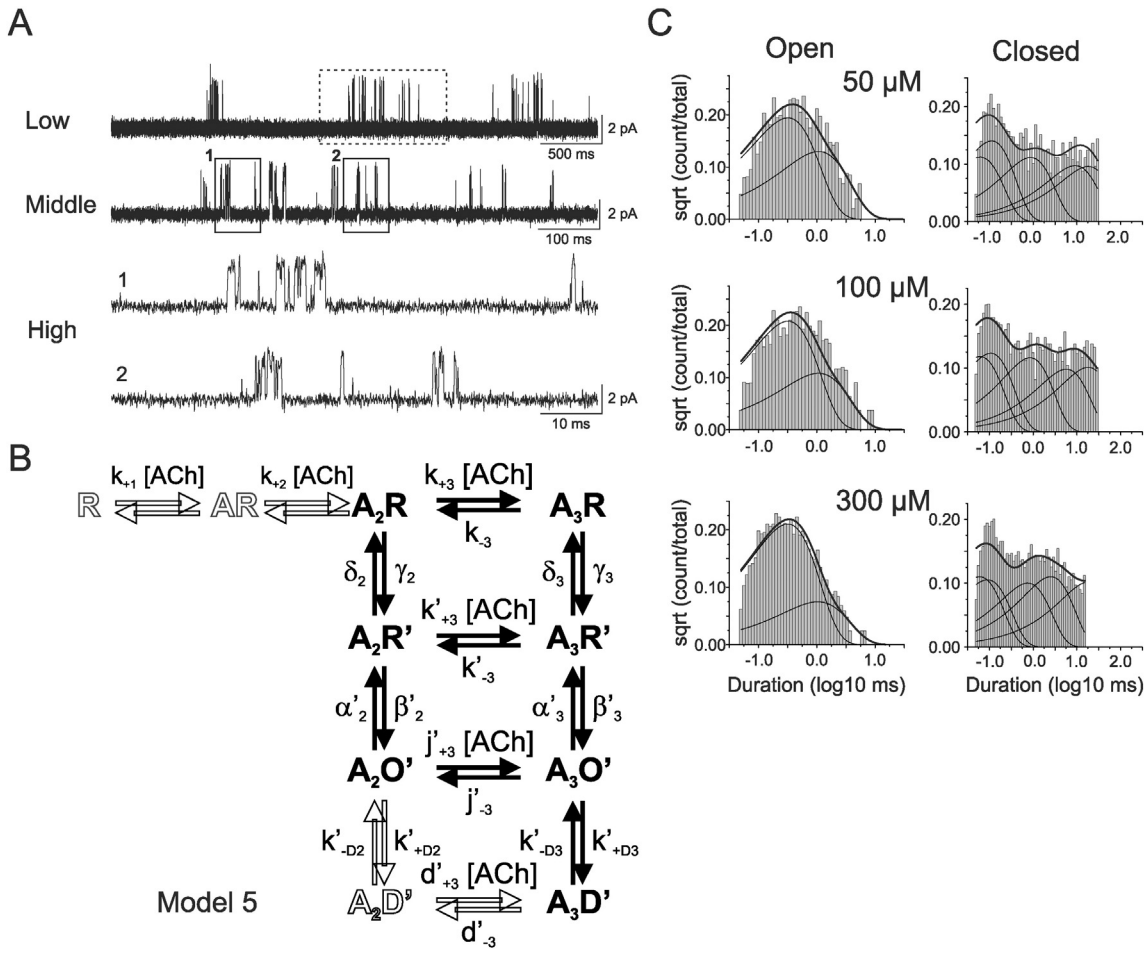

Fig. 6. Kinetic analysis of HC channel. (A) Single-channel recordings of clusters activity at 3 different time resolutions. Dash box in upper trace delimits a cluster that is exposed with higher temporal resolution in the middle panel. Closed-numbered boxes delimit intracluster periods that exhibited in the lower traces 1 and 2 with higher temporal resolution. ACh concentration: 100 μM. (B) Kinetic model which contains an intermediate primed state in between resting and open states for the diliganded and triliganded receptor. Bold letters and arrows indicate the states used for fitting while white-filled letters and arrow indicates possible pathways that were not used for kinetic modeling. (C) Experimental open- and closed-time histograms with the superimposed fit obtained from the model using the kinetic parameters calculated by QuB software.

maximum current [21,22,62]. HC channel also has the 2 high-affinity BSs structurally identical to LC channel besides the low-affinity BS, $\alpha4^{(+)}/\alpha4^{(-)}$. Thus, it would activate at low concentrations of ACh by binding to the 2 high-affinity sites and when agonist concentration is increased, it will bind to the third site (Fig. 5B, Scheme 2). [19–21,23,43]. Based on our data for the LC channel activation and published data, binding of ACh to the $\alpha4^{(+)}/\beta2^{(-)}$ site in HC channel would generate a low efficacious activation. This also has been observed for the concatenated receptor [27,47]. Binding of the agonist to the $\alpha4^{(+)}/\alpha4^{(-)}$ promotes full activation of the receptor, increasing the amount of current generated by the receptor molecules [21–23,62]. At the single-channel level, this improved activation is correlated with the presence of clusters generated by the activation of the receptor. We assume that cluster activities are generated when the receptor binds the third agonist and analyzed several kinetic models to describe activation kinetics. The pattern of closures is complex and indicates that, compared to muscle-type nAChR, the efficacy of activation is much lower [59]. When we consider the total opening time inside a cluster for muscle nAChR activated by an efficacious agonist is close to 99%, while here, this time is close to 10% when we consider the whole clusters and approximately 40% if we consider burst of activations inside clusters. Our kinetic analysis indicates that to open the channel, the receptor must reach a primed state that precludes opening, indicating an explanation to the action of the high-affinity sites as partial agonists. The transition between the closed states to the primed states is much faster in the triliganded receptor compared to the diliganded receptor (around 18 times). In consequence, opening of the receptor with two ACh bounded proceeds very slowly and could probably explain why these receptor subtypes desensitize even in the presence of very low concentrations of agonist [42]. Once the receptor reaches the primed state, gating of the bi- or triliganded receptor is similar, with even a faster opening rate for the diliganded than the triliganded state. Also the stability of the diliganded open state is higher than the triliganded open state (Table 1), reinforcing the idea that the third agonist molecule would act more as a modulator which favors the transition from the resting to the primed state. Once the receptor is primed, it would be efficiently coupled to opening, no matter if it has 2 or 3 agonist molecules bound. Primed states also have been determined for members of the Cys-loop family, like serotonin receptor, $GABA_A$ receptor and muscle nAChRs [30,31,63] and this state would be responsible for the action of several compounds as partial agonists [32,64]. Structurally, nAChRs primed states would correspond to the movement of C-loop from uncapped to capped position in the binding site upon binding of the agonist [65,66], as it has been demonstrated for muscle nAChR [30]. Our study suggests that binding of ACh to its low affinity binding site is necessary to overcome this conformational change necessary for channel gating.

5. Conclusions

The main finding of our study is the determination of kinetic parameters for the activation of the low-sensitivity $\alpha4\beta2$ receptor. Our results

Table 1
Kinetic parameters for nAChR $(\alpha4)_3(\beta2)_2$ activated by ACh. Kinetic parameters correspond to the activation schemes shown in Figs. 5C and 6C and are the result of a global fit of data obtained over a range of ACh concentrations. Standard errors are shown. Equilibrium constants (indicated with bold numbers) are K for association to resting state, K′ for association to the primed state, J for association to open state, F for primed state, θ for gating and K_D for desensitization. Asterisks indicate equilibrium constants that are not compatible with observed values.

	Classical models				Primed models	
	Model 1	Model 2	Model 3	Model 4	Model 5	Model 6
k_{+3} (μM^{-1} s^{-1})	11 ± 1	15 ± 1	11 ± 1	11 ± 1	2.3 ± 0.5	2.5 ± 0.6
k_{-3} (s^{-1})	2944 ± 167	3341 ± 167	2886 ± 157	2940 ± 149	284 ± 25	292 ± 27
K_3 (μM^{-1})	**277.7**	**222.7**	**258.5**	**263**	**123**	**117**
k'_{+3} (μM^{-1} s^{-1})	–	–	–	–	2.47E-04	11 ± 3
k'_{-3} (s^{-1})	–	–	–	–	1.90E-06	408 ± 78
K'_3 (μM^{-1})	–	–	–	–	**7.66E-03**	**37**
j_{+3} or j'_{+3} (μM^{-1} s^{-1})	14 ± 1	15 ± 1	14 ± 1	16 ± 1	1.5 ± 0.3	–
j_{-3} or j'_{-3} (s^{-1})	356 ± 55	303 ± 46	377 ± 60	354 ± 49	162 ± 23	–
J_3 or J'_3 (μM^{-1})	**25**	**20**	**27**	**22**	**108**	–
γ_2 (s^{-1})	–	–	–	–	37 ± 9	41 ± 10
δ_2 (s^{-1})	–	–	–	–	1921 ± 184	2056 ± 208
F_2	–	–	–	–	**0.019**	**0.019**
γ_3 (s^{-1})	–	–	–	–	1446 ± 96	1454 ± 97
δ_3 (s^{-1})	–	–	–	–	4197 ± 290	4213 ± 317
F_3	–	–	–	–	**0.34**	**0.34**
β_2 or β'_2 (s^{-1})	43 ± 11	12 ± 9	–	–	9040 ± 660	8952 ± 726
α_2 or α'_2 (s^{-1})	6.4E-05 ± 5E-06	8.6E-05 ± 3E-06	–	–	1430 ± 65	1552 ± 73
θ_2 or θ'_2	**6.7E + 05***	**1.4E + 05***	–	–	**6.3**	**5.8**
β_3 or β'_3 (s^{-1})	6550 ± 279	6919 ± 290	6438 ± 274	5992 ± 239	5392 ± 312	5178 ± 322
α_3 or α'_3 (s^{-1})	2772 ± 96	2480 ± 71	2693 ± 89	2605 ± 70	3207 ± 72	3247 ± 85
θ_3 or θ'_3	**2.36**	**2.79**	**2.39**	**2.3**	**1.7**	**1.6**
k_{+D2} or k'_{+D2} (s^{-1})	207 ± 32	–	196 ± 39	–	–	–
k_{-D2} or k'_{-D2} (s^{-1})	38 ± 3	–	41 ± 5	–	–	–
K_{D2} or K'_{D2}	**0.18**	–	**0.21**	–	–	–
k_{+D3} or k'_{+D3} (s^{-1})	1014 ± 35	1054 ± 30	991 ± 31	1002 ± 30	679 ± 48	699 ± 51
k_{-D3} or k'_{-D3} (s^{-1})	51 ± 1	52 ± 1	50 ± 1	52 ± 1	54 ± 2	53 ± 2
K_{D3} or K'_{D3}	**19.880**	**0.049**	**0.051**	**0.052**	**0.080**	**0.070**

indicate the presence of an intermediate state, between resting and open conformation of the receptor. Binding of the third molecule to the low-affinity BS increases the efficacy of receptor activation by favoring the transition between resting and intermediate state, named primed.

Transparency Document

The Transparency document associated with this article can be found, in the online version.

Acknowledgements

This work was supported by funds from Agencia Nacional de Promoción Científica y Tecnológica (PICT2011 N°0251) and CONICET (PIP2012-2014). EPB was holder of an undergraduate fellowship from Comisión de Investigaciones Científicas (2014–2015).

Authors are grateful to Dr. Cecilia Bouzat for providing access to patch-clamp equipment and Dr. Jeremías Corradi for helpful advice on kinetic modeling.

References

[1] E.X. Albuquerque, E.F. Pereira, M. Alkondon, S.W. Rogers, Mammalian nicotinic acetylcholine receptors: from structure to function, Physiol. Rev. 89 (2009) 73–120.
[2] N.S. Millar, C. Gotti, Diversity of vertebrate nicotinic acetylcholine receptors, Neuropharmacology 56 (2009) 237–246.
[3] S.M. Sine, A.G. Engel, Recent advances in Cys-loop receptor structure and function, Nature 440 (2006) 448–455.
[4] P.H. Barry, J.W. Lynch, Ligand-gated channels, IEEE Trans. Nanobiosci. 4 (2005) 70–80.
[5] M.R. Picciotto, B.J. Caldarone, D.H. Brunzell, V. Zachariou, T.R. Stevens, S.L. King, Neuronal nicotinic acetylcholine receptor subunit knockout mice: physiological and behavioral phenotypes and possible clinical implications, Pharmacol. Ther. 92 (2001) 89–108.
[6] M. Zoli, F. Pistillo, C. Gotti, Diversity of native nicotinic receptor subtypes in mammalian brain, Neuropharmacol. Part B 96 (2015) 302–311.
[7] C.G. Baddick, M.J. Marks, An autoradiographic survey of mouse brain nicotinic acetylcholine receptors defined by null mutants, Biochem. Pharmacol. 82 (2011) 828–841.
[8] E.D. Levin, Complex relationships of nicotinic receptor actions and cognitive functions, Biochem. Pharmacol. 86 (2013) 1145–1152.
[9] M. Grupe, M. Grunnet, J.F. Bastlund, A.A. Jensen, Targeting α4β2 nicotinic acetylcholine receptors in central nervous system disorders: perspectives on positive allosteric modulation as a therapeutic approach, Basic Clin. Pharmacol. Toxicol. 116 (2015) 187–200.
[10] C. Gotti, M. Zoli, F. Clementi, Brain nicotinic acetylcholine receptors: native subtypes and their relevance, Trends Pharmacol. Sci. 27 (2006) 482–491.
[11] M.J. Higley, M.R. Picciotto, Neuromodulation by acetylcholine: examples from schizophrenia and depression, Curr. Opin. Neurobiol. 29 (2014) 88–95.
[12] A.A. Jensen, B. Frølund, T. Liljefors, P. Krogsgaard-Larsen, Neuronal nicotinic acetylcholine receptors: structural revelations, target identifications, and therapeutic inspirations, J. Med. Chem. 48 (2005) 4705–4745.
[13] C. Lena, J. Changeux, C. Mulle, Evidence for "preterminal" nicotinic receptors on GABAergic axons in the rat interpeduncular nucleus, J. Neurosci. 13 (1993) 2680–2688.
[14] T.D. McClure-Begley, N.M. King, A.C. Collins, J.A. Stitzel, J.M. Wehner, C.M. Butt, Acetylcholine-stimulated [3H]GABA release from mouse brain synaptosomes is modulated by α4β2 and α4α5β2 nicotinic receptor subtypes, Mol. Pharmacol. 75 (2009) 918–926.
[15] S. Zappettini, M. Grilli, A. Salamone, E. Fedele, M. Marchi, Pre-synaptic nicotinic receptors evoke endogenous glutamate and aspartate release from hippocampal synaptosomes by way of distinct coupling mechanisms, Br. J. Pharmacol. 161 (2010) 1161–1171.
[16] W.M. Howe, J. Ji, V. Parikh, S. Williams, E. Mocaer, C. Trocme-Thibierge, M. Sarter, Enhancement of attentional performance by selective stimulation of α4β2* nAChRs: underlying cholinergic mechanisms, Neuropsychopharmacology 35 (2010) 1391–1401.
[17] D.J. Anderson, J. Malysz, J.H. Grønlien, R. El Kouhen, M. Håkerud, C. Wetterstrand, C.A. Briggs, M. Gopalakrishnan, Stimulation of dopamine release by nicotinic acetylcholine receptor ligands in rat brain slices correlates with the profile of high, but not low, sensitivity α4β2 subunit combination, Biochem. Pharmacol. 78 (2009) 844–851.
[18] M.E. Nelson, A. Kuryatov, C.H. Choi, Y. Zhou, J. Lindstrom, Alternate stoichiometries of α4β2 nicotinic acetylcholine receptors, Mol. Pharmacol. 63 (2003) 332–341.
[19] M. Moroni, R. Zwart, E. Sher, B.K. Cassels, I. Bermudez, α4β2 nicotinic receptors with high and low acetylcholine sensitivity: pharmacology, stoichiometry, and sensitivity to long-term exposure to nicotine, Mol. Pharmacol. 70 (2006) 755–768.
[20] A.L. Carbone, M. Moroni, P.J. Groot-Kormelink, I. Bermudez, Pentameric concatenated $(\alpha4)_2(\beta2)_3$ and $(\alpha4)_3(\beta2)_2$ nicotinic acetylcholine receptors: subunit arrangement determines functional expression, Br. J. Pharmacol. 156 (2009) 970–981.

[21] K. Harpsoe, P.K. Ahring, J.K. Christensen, M.L. Jensen, D. Peters, T. Balle, Unraveling the high- and low-sensitivity agonist responses of nicotinic acetylcholine receptors, J. Neurosci. 31 (2011) 10759–10766.

[22] L.M. Lucero, M.M. Weltzin, J.B. Eaton, J.F. Cooper, J.M. Lindstrom, R.J. Lukas, P. Whiteaker, Differential α4(+)/(−)β2 agonist binding site contributions to α4β2 nicotinic acetylcholine receptor function within and between isoforms, J. Biol. Chem. (2015).

[23] S. Mazzaferro, N. Benallegue, A. Carbone, F. Gasparri, R. Vijayan, P.C. Biggin, M. Moroni, I. Bermudez, Additional acetylcholine (ACh) binding site at α4/α4 interface of $(\alpha4\beta2)_2\alpha4$ nicotinic receptor influences agonist sensitivity, J. Biol. Chem. 286 (2011) 31043–31054.

[24] P. Aracri, A. Amadeo, M.E. Pasini, U. Fascio, A. Becchetti, Regulation of glutamate release by heteromeric nicotinic receptors in layer V of the secondary motor region (Fr2) in the dorsomedial shoulder of prefrontal cortex in mouse, Synapse 67 (2013) 338–357.

[25] H. Matsubayashi, A. Inoue, T. Amano, T. Seki, Y. Nakata, M. Sasa, N. Sakai, Involvement of α7- and α4β2-type postsynaptic nicotinic acetylcholine receptors in nicotine-induced excitation of dopaminergic neurons in the substantia nigra: a patch clamp and single-cell PCR study using acutely dissociated nigral neurons, Mol. Brain Res. 129 (2004) 1–7.

[26] M. Grupe, G. Paolone, A.A. Jensen, K. Sandager-Nielsen, M. Sarter, M. Grunnet, Selective potentiation of $(\alpha4)3(\beta2)2$ nicotinic acetylcholine receptors augments amplitudes of prefrontal acetylcholine- and nicotine-evoked glutamatergic transients in rats, Biochem. Pharmacol. 86 (2013) 1487–1496.

[27] J. Wang, A. Kuryatov, A. Sriram, Z. Jin, T.M. Kamenecka, P.J. Kenny, J. Lindstrom, An accessory agonist binding site promotes activation of α4β2* nicotinic acetylcholine receptors, J. Biol. Chem. 290 (2015) 13907–13918.

[28] C.Z. Zhu, C.-l. Chin, N.R. Rustay, C. Zhong, J. Mikusa, P. Chandran, A. Salyers, E. Gomez, G. Simler, L.G. Lewis, D. Gauvin, S. Baker, M. Pai, A. Tovcimak, J. Brown, V. Komater, G.B. Fox, M.W. Decker, P.B. Jacobson, M. Gopalakrishnan, C.-H. Lee, P. Honore, Potentiation of analgesic efficacy but not side effects: Co-administration of an α4β2 neuronal nicotinic acetylcholine receptor agonist and its positive allosteric modulator in experimental models of pain in rats, Biochem Pharmacol 82 (2011) 967–976.

[29] D.B. Timmermann, K. Sandager-Nielsen, T. Dyhring, M. Smith, A.M. Jacobsen, E. Nielsen, M. Grunnet, J.K. Christensen, D. Peters, K. Kohlhaas, G.M. Olsen, P.K. Ahring, Augmentation of cognitive function by NS9283, a stoichiometry-dependent positive allosteric modulator of α2- and α4-containing nicotinic acetylcholine receptors, Br. J. Pharmacol. 167 (2012) 164–182.

[30] N. Mukhtasimova, W.Y. Lee, H.L. Wang, S.M. Sine, Detection and trapping of intermediate states priming nicotinic receptor channel opening, Nature 459 (2009) 451–454.

[31] R. Lape, A.J. Plested, M. Moroni, D. Colquhoun, L.G. Sivilotti, The alpha1K276E startle disease mutation reveals multiple intermediate states in the gating of glycine receptors, J. Neurosci. 32 (2012) 1336–1352.

[32] J. Corradi, C. Bouzat, Unraveling mechanisms underlying partial agonism in 5-HT3A receptors, J. Neurosci. 34 (2014) 16865–16876.

[33] M. Szczot, M. Kisiel, M.M. Czyzewska, J.W. Mozrzymas, α1F64 residue at $GABA_A$ receptor binding site is involved in gating by influencing the receptor flipping transitions, J. Neurosci. 34 (2014) 3193–3209.

[34] W.S. Pear, G.P. Nolan, M.L. Scott, D. Baltimore, Production of high-titer helper-free retroviruses by transient transfection, Proc. Natl. Acad. Sci. U. S. A. 90 (1993) 8392–8396.

[35] G. Spitzmaul, F. Gumilar, J.P. Dilger, C. Bouzat, The local anaesthetics proadifen and adiphenine inhibit nicotinic receptors by different molecular mechanisms, Br. J. Pharmacol. 157 (2009) 804–817.

[36] D. Rayes, G. Spitzmaul, S.M. Sine, C. Bouzat, Single-channel kinetic analysis of chimeric alpha7-5HT3A receptors, Mol. Pharmacol. 68 (2005) 1475–1483.

[37] G. Spitzmaul, J. Corradi, C. Bouzat, Mechanistic contributions of residues in the M1 transmembrane domain of the nicotinic receptor to channel gating, Mol. Membr. Biol. 21 (2004) 39–50.

[38] F. Qin, A. Auerbach, F. Sachs, Estimating single-channel kinetic parameters from idealized patch-clamp data containing missed events, Biophys. J. 70 (1996) 264–280.

[39] G. Zhu, Y. Zhang, H. Xu, C. Jiang, Identification of endogenous outward currents in the human embryonic kidney (HEK 293) cell line, J. Neurosci. Methods 81 (1998) 73–83.

[40] A. Varghese, E.M. Tenbroek, J. Coles Jr., D.C. Sigg, Endogenous channels in HEK cells and potential roles in HCN ionic current measurements, Prog. Biophys. Mol. Biol. 90 (2006) 26–37.

[41] B. Buisson, M. Gopalakrishnan, S.P. Arneric, J.P. Sullivan, D. Bertrand, Human α4β2 neuronal nicotinic acetylcholine receptor in HEK 293 cells: a patch-clamp study, J. Neurosci. 16 (1996) 7880–7891.

[42] K.G. Paradiso, J.H. Steinbach, Nicotine is highly effective at producing desensitization of rat α4β2 neuronal nicotinic receptors, J. Physiol. 553 (2003) 857–871.

[43] P. Li, J.H. Steinbach, The neuronal nicotinic α4β2 receptor has a high maximal probability of being open, Br. J. Pharmacol. 160 (2010) 1906–1915.

[44] A. Kuryatov, V. Gerzanich, M. Nelson, F. Olale, J. Lindstrom, Mutation causing autosomal dominant nocturnal frontal lobe epilepsy alters Ca^{2+} permeability, conductance, and gating of human α4β2 nicotinic acetylcholine receptors, J. Neurosci. 17 (1997) 9035–9047.

[45] B. Buisson, D. Bertrand, Chronic exposure to nicotine upregulates the human α4β2 nicotinic acetylcholine receptor function, J. Neurosci. 21 (2001) 1819–1829.

[46] L. Curtis, B. Buisson, S. Bertrand, D. Bertrand, Potentiation of human alpha4beta2 neuronal nicotinic acetylcholine receptor by estradiol, Mol. Pharmacol. 61 (2002) 127–135.

[47] S. Mazzaferro, F. Gasparri, K. New, C. Alcaino, M. Faundez, P. Iturriaga Vasquez, R. Vijayan, P.C. Biggin, I. Bermudez, Non-equivalent ligand selectivity of agonist sites in $(\alpha4\beta2)_2\alpha4$ nicotinic acetylcholine receptors: a key determinant of agonist efficacy, J. Biol. Chem. 289 (2014) 21795–21806.

[48] D. Colquhoun, R. Lape, Perspectives on: conformational coupling in ion channels: allosteric coupling in ligand-gated ion channels, J. Gen. Physiol. 140 (2012) 599–612.

[49] V. Burzomato, M. Beato, P.J. Groot-Kormelink, D. Colquhoun, L.G. Sivilotti, Single-channel behavior of heteromeric alpha1beta glycine receptors: an attempt to detect a conformational change before the channel opens, J. Neurosci. 24 (2004) 10924–10940.

[50] M. Ballivet, P. Nef, S. Couturier, D. Rungger, C.R. Bader, D. Bertrand, E. Cooper, Electrophysiology of a chick neuronal nicotinic acetylcholine receptor expressed in Xenopus oocytes after cDNA injection, Neuron 1 (1988) 847–852.

[51] R.L. Papke, J. Boulter, J. Patrick, S. Heinemann, Single-channel currents of rat neuronal nicotinic acetylcholine receptors expressed in xenopus oocytes, Neuron 3 (1989) 589–596.

[52] E. Cooper, S. Couturier, M. Ballivet, Pentameric structure and subunit stoichiometry of a neuronal nicotinic acetylcholine receptor, Nature 350 (1991) 235–238.

[53] P. Charnet, C. Labarca, B.N. Cohen, N. Davidson, H.A. Lester, G. Pilar, Pharmacological and kinetic properties of α4β2 neuronal nicotinic acetylcholine receptors expressed in *Xenopus* oocytes, J. Physiol. 450 (1992) 375–394.

[54] E.F. Pereira, M. Alkondon, S. Reinhardt, A. Maelicke, X. Peng, J. Lindstrom, P. Whiting, E.X. Albuquerque, Physostigmine and galanthamine: probes for a novel binding site on the α4β2 subtype of neuronal nicotinic acetylcholine receptors stably expressed in fibroblast cells, J. Pharmacol. Exp. Ther. 270 (1994) 768–778.

[55] J. Ramirez-Latorre, C.R. Yu, X. Qu, F. Perin, A. Karlin, L. Role, Functional contributions of α5 subunit to neuronal acetylcholine receptor channels, Nature 380 (1996) 347–351.

[56] J.A. Peters, T.G. Hales, J.J. Lambert, Molecular determinants of single-channel conductance and ion selectivity in the Cys-loop family: insights from the 5-HT3 receptor, Trends Pharmacol. Sci. 26 (2005) 587–594.

[57] T.G. Hales, J.I. Dunlop, T.Z. Deeb, J.E. Carland, S.P. Kelley, J.J. Lambert, J.A. Peters, Common determinants of single channel conductance within the large cytoplasmic loop of 5-hydroxytryptamine type 3 and $\alpha_4\beta_2$ nicotinic acetylcholine receptors, J. Biol. Chem. 281 (2006) 8062–8071.

[58] S.M. Sine, T. Claudio, F.J. Sigworth, Activation of Torpedo acetylcholine receptors expressed in mouse fibroblasts. Single channel current kinetics reveal distinct agonist binding affinities, J. Gen. Physiol. 96 (1990) 395–437.

[59] Y. Zhang, J. Chen, A. Auerbach, Activation of recombinant mouse acetylcholine receptors by acetylcholine, carbamylcholine and tetramethylammonium, J. Physiol. 486 (1995) 189–206.

[60] G. Akk, A. Auerbach, Activation of muscle nicotinic acetylcholine receptor channels by nicotinic and muscarinic agonists, Br. J. Pharmacol. 128 (1999) 1467–1476.

[61] N. Benallegue, S. Mazzaferro, C. Alcaino, I. Bermudez, The additional ACh binding site at the α4(+)/α4(−) interface of the $(\alpha4\beta2)_2\alpha4$ nicotinic ACh receptor contributes to desensitization, Br. J. Pharmacol. 170 (2013) 304–316.

[62] J.B. Eaton, L.M. Lucero, H. Stratton, Y. Chang, J.F. Cooper, J.M. Lindstrom, R.J. Lukas, P. Whiteaker, The unique α4(+)/(−)α4 agonist binding site in $(\alpha4)_3(\beta2)_2$ subtype nicotinic acetylcholine receptors permits differential agonist desensitization pharmacology versus the $(\alpha4)_2(\beta2)_3$ subtype, J. Pharmacol. Exp. Ther. 348 (2014) 46–58.

[63] J. Corradi, F. Gumilar, C. Bouzat, Single-channel kinetic analysis for activation and desensitization of homomeric 5-HT_3A receptors, Biophys. J. 97 (2009) 1335–1345.

[64] R. Lape, D. Colquhoun, L.G. Sivilotti, On the nature of partial agonism in the nicotinic receptor superfamily, Nature 454 (2008) 722–727.

[65] S.B. Hansen, G. Sulzenbacher, T. Huxford, P. Marchot, P. Taylor, Y. Bourne, Structures of aplysia AChBP complexes with nicotinic agonists and antagonists reveal distinctive binding interfaces and conformations, EMBO J. 24 (2005) 3635–3646.

[66] P.H. Celie, S.E. van Rossum-Fikkert, W.J. van Dijk, K. Brejc, A.B. Smit, T.K. Sixma, Nicotine and carbamylcholine binding to nicotinic acetylcholine receptors as studied in AChBP crystal structures, Neuron 41 (2004) 907–914.